

Article

A Comparative Study of Different Fingertips on the Object Pulling Forces in Robotic Gripper Jaws

Marcin Białek *  and Dominik Rybarczyk 

Division of Mechatronic Devices, Institute of Mechanical Technology, Faculty of Mechanical Engineering, Poznan University of Technology, 60-965 Poznan, Poland

* Correspondence: marcin.bialek@put.poznan.pl

Abstract: This paper presents a comparative study of the use of different fingertips in robotic gripper jaws with respect to measuring the pulling force of selected shaped objects from their grasp. The authors built a dedicated test stand and provided methodology to evaluate it. The authors' innovative approach was to design accessory-controlled jaws for the base of the Robotiq 2F-140 gripper. For the study, rigid structures—flexible soft cushions filled with air and magnetorheological fluid (MRF)—were developed for the jaw. In this way, comparable measurement results were obtained in terms of the structure of the gripper set-up. The secondary purpose of the study was to demonstrate the potential of the soft cushions that are adaptable to the shape of a gripped object. As a result, an adaptive structure was obtained that allows object pulling forces that are comparable to rigid fingertips. In doing so, this does not damage the surface of any of the interacting components. The cushions were made of thermoplastic polyurethane (TPU) formed using 3D printing technology. The results obtained during the implementation of this research may be beneficial for comparing gripper capabilities; thus, they can contribute to advances in smart devices and many industrial fields, including robotics and bioengineering.

Keywords: parallel gripper; thermoplastic polyurethane (TPU); magnetorheological fluid (MRF); 3D printing; grasping



Citation: Białek, M.; Rybarczyk, D. A Comparative Study of Different Fingertips on the Object Pulling Forces in Robotic Gripper Jaws. *Appl. Sci.* **2023**, *13*, 1247. <https://doi.org/10.3390/app13031247>

Academic Editors: Josip Musić and Vladan Papić

Received: 23 December 2022

Revised: 12 January 2023

Accepted: 13 January 2023

Published: 17 January 2023



Copyright: © 2023 by the authors. Licensee MDPI, Basel, Switzerland. This article is an open access article distributed under the terms and conditions of the Creative Commons Attribution (CC BY) license (<https://creativecommons.org/licenses/by/4.0/>).

1. Introduction

Soft gripping structures are a popular research topic due to the many technologies [1] in which they are used. Their structural compliance limits the precision of object manipulation and force exertion [2], which in turn, features rigid grippers. Because of their potential, scientists are conducting research to increase their gripping force in the first instance. This includes, for example, interference with the structure of silicone fingers [3,4], a topological optimization of the design of pneumatic bending actuators [5], experiments with the texture of gripping tips [6], or innovative control based on machine learning algorithms [7]. The application of a given gripper is also very important, which can limit its dimensions [8]. An effective way to combine the advantages of soft and rigid structures is to create a hybrid of both. Currently, the origami-based structure provides grip stability and dexterity, an improved lifting force of delicate objects, and soft bladder pressure-sensing, which is a popular topic [9]. Soft structures require soft materials such as silicone [4–7], latex (e.g., a balloon [9–11]), or polyurethane films [12]. Thermoplastic polyurethane (TPU), which can be 3D printed, is an excellent option [13,14]. It finds its application, for example, in functional clothing and technical textiles as additional protection for the important parts of the body that are prone to injury [15]. The use of 3D printing technology, in this case, makes it possible to create monolithic structures of varying thicknesses or heights, and this has a huge impact on the flexibility of, not so much the material itself, but the components that are made of it. A very good example is the anthropomorphic hand, which has a smaller cross-sectional area for bending spots [16]. Therefore, this is an interesting alternative to MRF

reservoirs that are made of cast silicone [17] in the form of a nitrile rubber pouch [18–20]. The examples demonstrate the interest of the scientific community in the potential use of magnetorheology in robotic grippers [17–27]. To compare and test the applicability of solutions based on flexible magnetorheological fluid (MRF) cushions, the authors conducted an analysis of the ways in which the gripper force is often measured. In most cases, the authors of a given design or control solution rely on measurements using a force gauge. Sometimes, they perform experiments to lift objects of a known weight [4] or perform payload tests using weights [5]. For large diameter jamming grippers, a cylindrical indenter is used, which is pulled out in the opposite direction after a membrane is plunged [19,28]. In addition to real objects, such as fruits or bottles, researchers also use simple prisms, such as a column, sphere or cube [3,6,8,9,20]. The available articles accurately present the test stands on which pulling-out force measurements have been carried out. Most often, this is performed by connecting a grasped object to a force gauge. In this case, the axially of the measurement is not retained. Additionally, the grippers are not rigidly fixed (for example, they are mounted on a robot), and this type of approach makes it difficult to later cross-reference the results. This is because the conditions are difficult to reproduce; however, the authors of this article identified an opportunity to introduce some systematization in the measurement methodology. For example, the potential possibility of comparing different variants of gripper components that can affect the gripping capabilities of a device was also noted. Therefore, considering the issues discussed, a test stand was proposed. The objects of the research covered in this article were the authors' fingertips, as the jaws in the Robotiq 2F-140 gripper used in robots such as the UR3e (Figure 1). The proposed solutions, using cushions, fit in the definition of hybrid soft-rigid gripping devices. The Robotiq 2F-140 gripper under study was operated in the parallel jaw mode by placing locking pins as shown in Figure 1. Section 2 proposes the fingertip configurations and grasped object geometries for comparative studies. The test stand and survey methodology are also presented. Section 3 presents the research results obtained, which are then discussed in Section 4, while Section 5 contains the conclusions of the experiments performed.

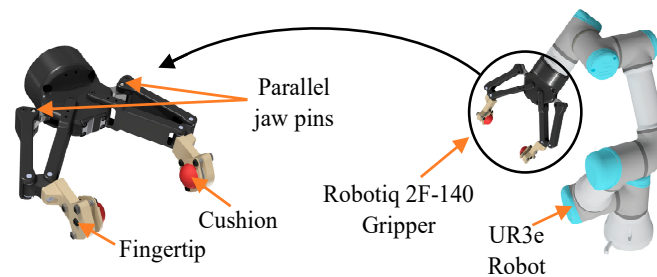


Figure 1. The research object: fingertips attached to the Robotiq 2F-140 gripper and an example of an application in the UR3e robot.

2. Materials and Methods

2.1. Manipulated Objects and Fingertips Characteristics

A key element of the research carried out was fingertips, particularly those that have MRF in their structure. Figure 2 shows schematically the configurations used in the tests. Starting from the left, each fingertip was tested on three differently-shaped objects made of 3D printed TPU. All the objects had the same height of 35 mm. Object 1 in the cross-section was a circle with a diameter of 24 mm. The other two objects had in a cross-section a hexagon fitted in a 24 mm diameter circle. Object 2 faced the fingertip with the side wall, while Object 3 faced the edge. The 24 mm dimension that was taken was based on the diameter of the cushion base minus its thickness. The tested fingertips consisted of base designs with a fingertip type 1 being rigid flat pads, fingertip type 2 being rigid flat pads with a 0.6 mm TPU layer, fingertip type 3 being soft air pads, and fingertip type 4 being soft MR fluid pads. The components were made of polylactic acid (PLA) using 3D printing. In the case of fingertip type 1 and the objects, there was, thus, contact between elements

made of the same material. Fingertip type 2 was enhanced with a TPU layer to indicate its advantages over fingertip type 1 and provide a comparability with the fingertip types 3 and 4. In the further sections of the article, the pads occurring in the fingertip types 3 and 4 will be referred to as cushions, which come in two geometric variants described in Section 2.2. The configurations of the individual pads are described in Section 2.3. Fingertip type 4 includes two MRFs from different manufacturers with the characteristic data shown in Table 1. The first was the LORD MRF-140CG [29], which was more than 10 years old. Its structure was much denser than the other as a result time. The second fluid was the ARUS MR TECH RHEOTEC+ with a high shear stress [30]. This fluid was more liquid-like (probably because of its age).

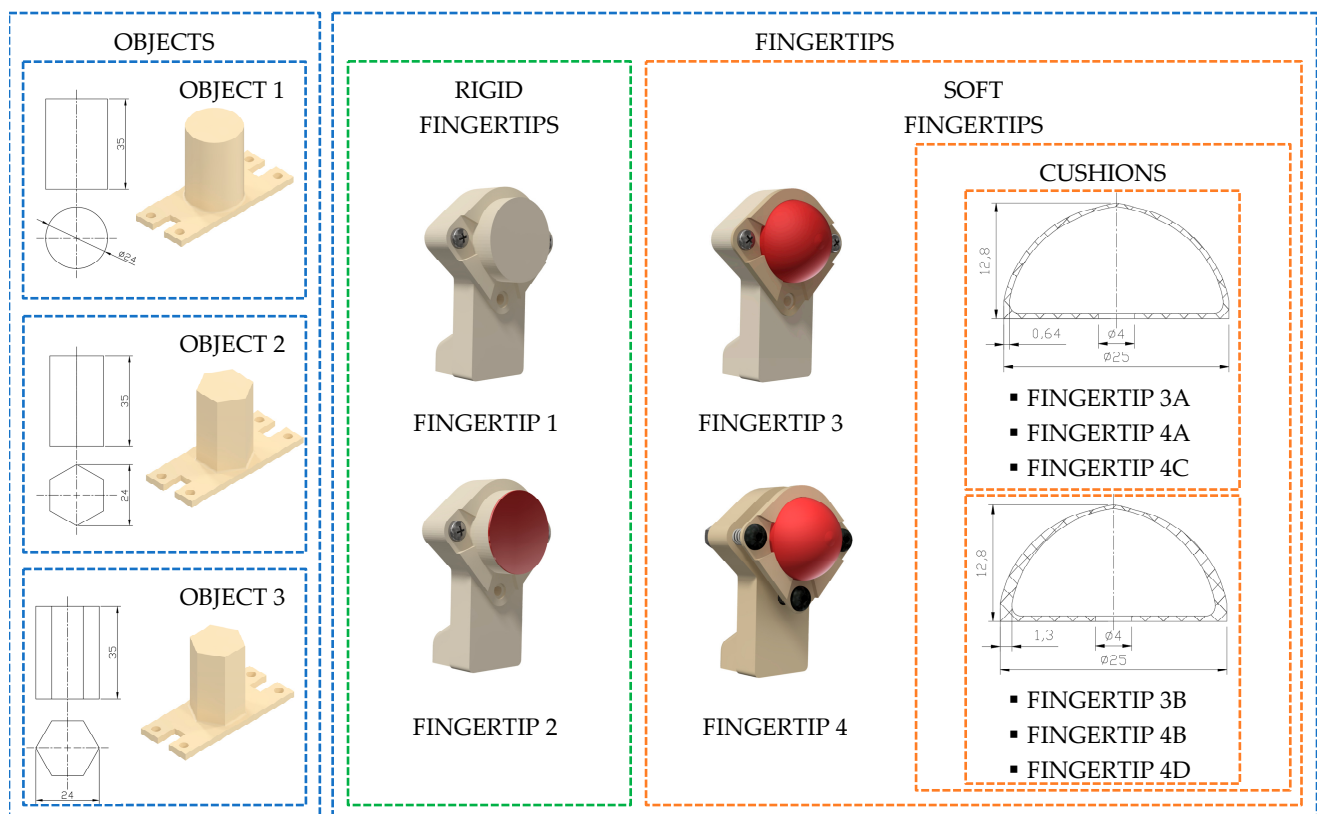


Figure 2. Chart illustrating the measurement array of grasped objects and designed fingertip configurations.

Table 1. Technical data for the lord MRF-140CG [29] and Arus MR Tech REOTEC+ [30] MRFs.

MR FLUID	LORD MRF-140CG	ARUS MR TECH RHEOTEC+
Viscosity, [Pa-s] (at 40 °C)	0.280 ± 0.070	0.240 ± 0.027
Density [g/cm ³]	3.54–3.74	3.1–3.3
Solids Content by Weight [%]	85.44	84
Maximum Yield Stress [kPa] at 180 kA/m	69 ± 5	~57
Age	~10 years	Factory new
Visible remarks	Dense, low oil content due to sedimentation	Liquid-like

2.2. 3D printed Cushion

It should be noted that the initial use of TPU as an MR cushion was presented by the authors in article [13]. A new aspect is the presented manufacturing method, printing conditions and procedure for closing a cushion prepared for mounting in a gripper jaw.

Additionally, in this article, the authors focused on the geometry of the semi-sphere by proposing the two cushions shown in Figure 2. Their common feature is a hole of 4 mm in diameter at the base. It was foreseen to insert MR fluids inside them using a syringe (Section 2.3). Both cushions also have the same height of 12.8 mm and a base diameter of 25 mm. Their tops are finished with an additional convexity allowing for a wider cross-section of the layer. This feature was implemented as a result of the analysis of model layers during the model cutting process in the PrusaSlicer 2.5.0 software [31]. The cushion found in the fingertip types 3A, 4A and 4C has a geometry that was developed based on the strategy of maintaining an equal wall thickness along the entire length of the vault arc. It is 0.64 mm. This cushion has greater elasticity compared to the other, mainly due to its thinner walls. At the same time, it is more difficult to manufacture. The fingertip types 3B, 4B and 4D use a cushion based on a fixed-layer geometry along the axis of rotation of the hemisphere. It is 1.3 mm wide and is formed over its entire height of 3 paths. This cushion is characterized by a greater stiffness, but at the same time guarantees a certain tightness of the cushion. The three-layer wall thickness provides for a minimum of two layers if one layer is discontinuous. It can be caused by the nozzle moving up a layer and is reduced using the option of an irregular seam position. Thus, the transition between the layers during printing takes place at random locations, avoiding the formation of a single seam on the wall. The print parameters and TPU material specifications are provided in Table 2. When working with TPU, it is necessary to properly prepare the filament prior to printing. This material is highly hygroscopic [32] and, therefore, prolonged exposure outside the sealed packaging affects the quality of the print. The authors dried the filament [15] at approximately 50 degrees Celsius for 30 min each time prior to the sample printing session. The reduction in print quality was caused by the evaporation of water from the moist filament during printing, making the flow of the melted polymer irregular [15]; thus, this caused a tendency for gaps and layer discontinuities to appear (Figure 3b,c).

Table 2. Three-dimensional printing parameters.

Printer	Model Nozzle Slicer	Prusa i3 MK3S+ 0.4 mm PrusaSlicer
Print Settings	Layer height Layers speed Flowrate Support material Fan Seam position	0.1 mm 20 mm/s 130% No Always on Random
Filament	manufacturer Product name Shore hardness Density	print-me.pl PrintMe Flex 20D 1.15 g/cm ³
Time of printing	Time of printing	1 h 22 m

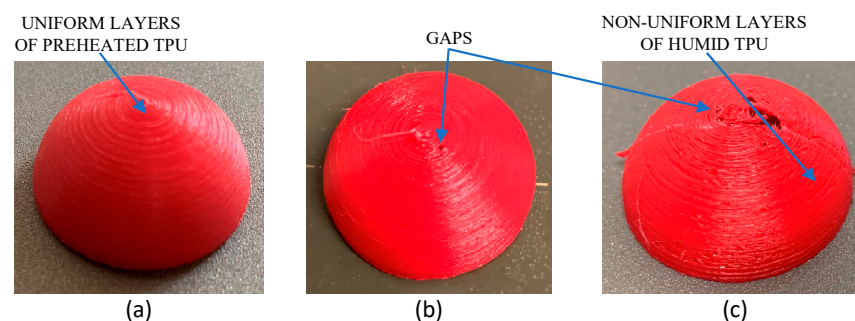


Figure 3. Three-dimensional printed TPU cushions: (a) correct—tight cushion with uniform layers, (b) faulty—untight cushion with a single gap at the top, and (c) faulty—leaky cushion with gaps and non-uniform layers.

2.3. Cushion Prototypes

In accordance with Figure 2, the authors carried out experiments on the eight cushion configurations shown in Table 3. The authors' aim was to demonstrate the differences in the properties of the cushions by comparing them in terms of the geometry and infill suggested in Section 2.2. Cushions no. 1 and 2 were air-filled. The remaining ones were manufactured according to the seven-step procedure shown in Figure 4. They were checked for tightness. In the first step, an appropriate volume of MRF was measured. For Cushions no. 7 and 8, a volume of 1 mL of glass microbeads with a diameter of 200–300 μm was prepared. This corresponded to 1.6 g. The idea of using microbeads was taken from the literature of [19,20]. Then, in Step 2, the syringe was inserted into the hole at the base of the cushion. By depressing the piston, the fluid flowed into the cushion. For Cushions no. 7 and 8, the microbeads were dropped first, using the syringe as a funnel. The cushion was thus prepared as is shown in Step 3 in Figure 4, where the syringe was gently removed. Step 4 was the preparation for closing and sealing the cushion. This was a combined process with Stage 5. It started by releasing the air trapped inside the cushion. By compressing the outer edges of the cushion, the liquid appeared in the 4 mm opening of the base. In Step 5, cyanoacrylate glue was spread around the perimeter of the hole as shown in Figure 4. To close the cushion, an 8 mm diameter disc was placed in the area of the hole. The entire procedure was carried out with a continuous cushion compression according to Step 4. As a result, once the glue had dried, the cushion shown in Step 6 was formed. Due to the release of air during the closing and sealing process, the cushions had a concave tip. In Step 7, the cushions were glued to the base with cyanoacrylate glue. Air removal had a positive effect on the cushioning behavior, as demonstrated by the research presented in article [13].

Table 3. Cushion prototypes.

Cushion Model	Fingertip Model	Infill	Infill Volume	Visible Remarks
Cushion 1	Fingertip 3A	AIR	-	hemisphere
Cushion 2	Fingertip 3B	AIR	-	hemisphere
Cushion 3	Fingertip 4A	MRF-140 CG	MRF: 2.6 mL	concave hemisphere
Cushion 4	Fingertip 4B	MRF-140 CG	MRF: 2.6 mL	concave hemisphere
Cushion 5	Fingertip 4C	RHEOTEC+	MRF: 2.6 mL	concave hemisphere
Cushion 6	Fingertip 4D	RHEOTEC+	MRF: 2.6 mL	concave hemisphere
Cushion 7	Fingertip 4C	RHEOTEC+ & microbeads	MRF: 1.6 mL Beads: 1 mL (1.6 g)	concave hemisphere
Cushion 8	Fingertip 4A	MRF-140 CG & microbeads	MRF: 1.6 mL Beads: 1 mL (1.6 g)	concave hemisphere

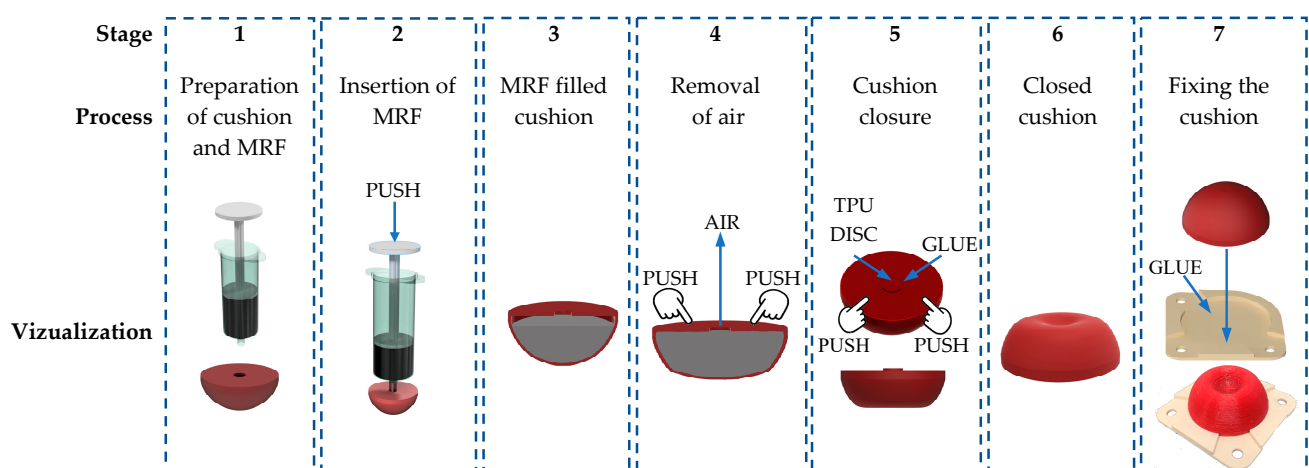


Figure 4. Scheme illustrating the seven-stage procedure of MRF cushion manufacturing.

2.4. Test Stand

To carry out the research, a dedicated test stand was built (Figure 5). The components were arranged on a levelled aluminum profile frame. As described in Figure 5a, the stand consisted of a linear drive that included a stepper motor, a leadscrew coupled to the motor and a HBM U9C-50N force sensor carriage. The test objects moved on a linear guide placed on a frame on a ball carriage. The carriage was connected to the force sensor via an inextensible wire. The authors experimented with a rigid connection using a threaded rod, but this type of solution brought a variable load into the measurements. In turn, all types of fishing line were too elastic and expanded their length when stretched. The second measuring device in the setup was a Panasonic HL-G112 laser distance sensor located on the side of the linear drive. The sensors and stepper motor were connected to the corresponding inputs of the PLC. The authors prepared their own program to operate the devices and collected measurement data using an interface in the B&R VNC Viewer [33]. Data were collected at a frequency of 1 kHz. The final key component of the test stand was the Robotiq 2F-140 gripper controlled by the UR3e Teach pendant with dedicated software. The fingertips discussed in Section 2.1 were replaced with the original jaws. The measurement procedure is discussed in Section 2.5.

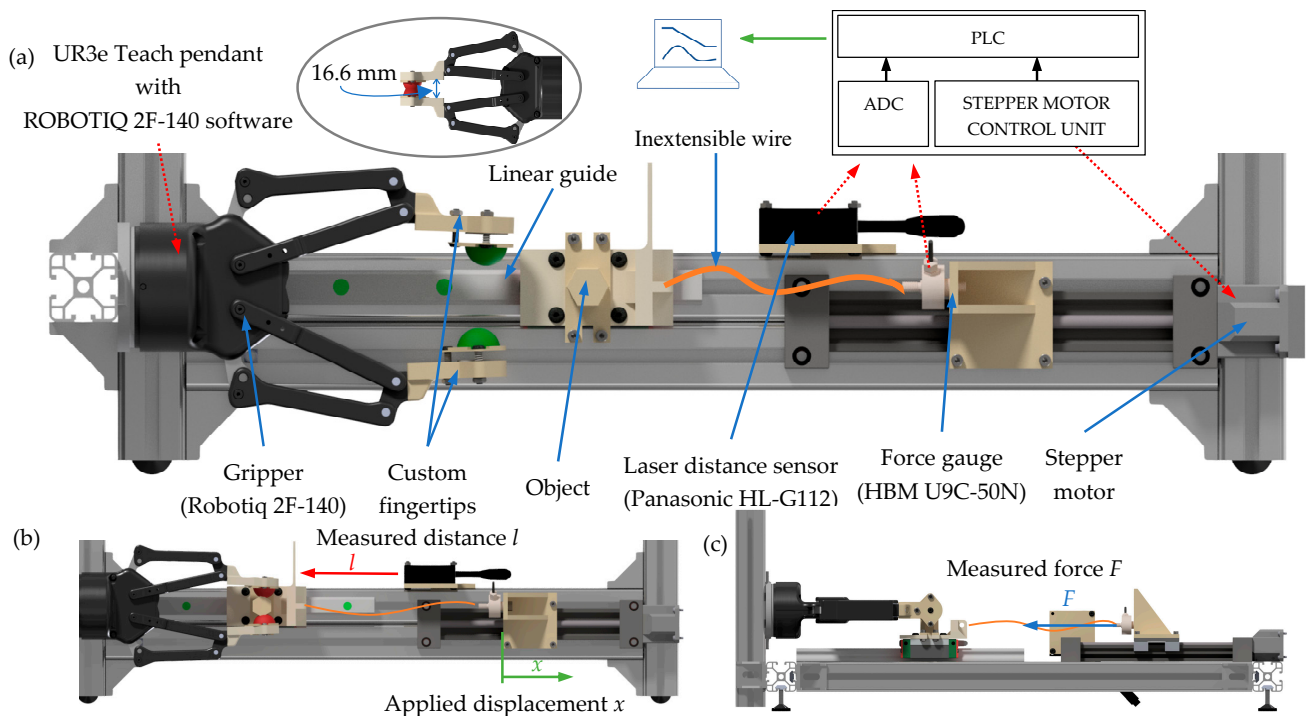


Figure 5. Scheme of the test stand: (a) top view with key components highlighted; (b) top view with the distance measured using the laser sensor and the displacement axis of the linear drive carriage indicated; (c) side view with the force measurement vector noted, with the top view of the gripper and the distance of 16.6 mm entered in the gripper settings.

2.5. Methodology

The aim of the tests carried out in this paper was to verify the force required to pull objects of defined shapes from the gripper fingertips by acting along one selected axis. An example of the measurement procedure and methodology is shown in Figure 6 for Cushion 1 (Table 3). It was started by placing the object in the area of the fingertip. This distance was taken as 90 mm from the face of the laser sensor (Figure 6). This corresponded to the position of the object close to the center of the fingertip. This approach ensured that the position of the object was repeatable in all fingertips and measurements. At this stage, the force sensor carriage was moved towards the gripper so that the inextensible

wire remained freely loose. Once the gripper jaws were closed, the measurement procedure started, and the object was pulled out at the constant speed of the linear drive. In Stage 2, the inextensible wire was strained to remove the slack that allowed the value of the force indicated by the sensor to be tare. In Stage 3, the wire was stretched, and the force began to rise. In Figure 6, the green line shows the course of the graph up to which the maximum force was reached. Pulling the object from the jaws continued up to the point indicated by the red line, which was completed in Step 4. Between the red line and the yellow line, the object lost contact with the fingertips and its release occurred. If the clamping force of the jaws was greater than zero, the object was pushed out by the pressing jaws caused by the removal of the obstacle from their area. Behind the yellow line, there was an increase in force of around 2.1 N. This value corresponded to the force that occurred when the carriage itself was pulled with the object and was the result of the friction of the carriage components along the linear guide. Typically, when the guide was cleaned, it was in the range of less than 4 N (see, e.g., Figure 7). In the case shown, this value was not reached due to an early termination of the movement. The final 6th stage was the opening of the jaws.

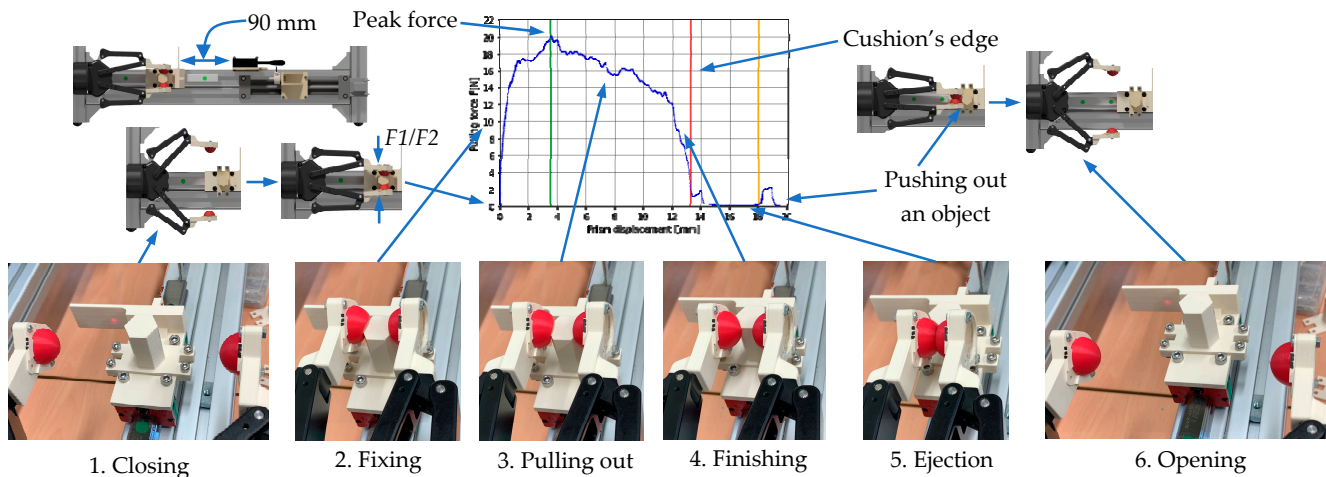


Figure 6. Chart illustrating a methodology of force measurement as a function of displacement for Fingertip type 3A and Object no. 3, along with individual stages of movement.

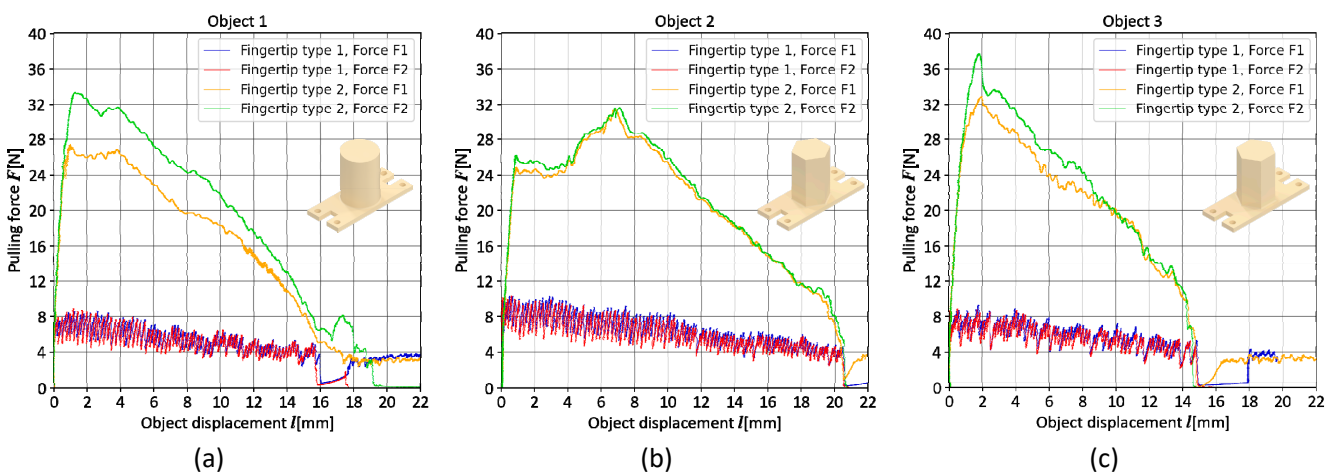


Figure 7. Measurement of the pulling force of an object from the fingertip types 1 and 2 as a function of its displacement for: (a) Object no. 1; (b) Object no. 2; (c) Object no. 3.

3. Results

The authors performed tests under different fingertip configurations as shown in Figure 2 for the two cases of actuation jaw force as shown in Table 4.

Table 4. Jaw force values applied during studies.

Force Description	UR3e Teach Pendant Designation	Actuation Force Value	Remarks
Force F1	0%	~15 N	Regrasp off: When an object is pulled out, the jaws remain in their position
Force F2	10%	~15 N	Regrasp on: When an object is pulled out, the jaws close

3.1. Fingertip Types 1 and 2

As the study showed, the use of a thin 0.6 mm TPU layer significantly affected the force achieved to pull objects from the jaws. In Fingertip type 1, the friction pair was PLA–PLA and the maximum forces achieved barely exceeded 10 N (Figure 7). For Fingertip type 2, the friction pair was PLA–TPU and the maximum forces observed were in the region of 38–39 N (Figure 7c). The consequence of the layer-by-layer printed wavy surface in Fingertip 1 was the large amplitudes of the force measurement in Figure 7. Regardless of the shape of the object being grasped, the same waveform characteristics were observed for this fingertip. The waveforms started with an overcoming of the static friction force, where a sudden increase and subsequent decrease in its value with the occurrence of kinetic friction were clearly visible. The difference was the cut-off point on the x-axis determined by the geometry of the object, and thus the length of its contact length with the fingertip. This was characterized by a sharp drop in force to 0 N. The measurements for Fingertip type 2 were affected by fewer oscillations. The first observation was the effect of an increase in the actuation force of the jaws on the objects, which with Objects no. 1 and 2 was expressed by an increase in the pull-out force. Due to the circle in the cross-section of Object no. 1, the fingertips slid along the curve (Figure 7a from an x-value of 16.5 mm). Object no. 2, because of its shape, offered the potential for a larger contact area than Objects no. 1 and no. 3. In this case, we observed a negligible effect of increasing the jaw actuation force on the pull-out force. The authors observed a certain tendency for the surface of the Fingertip types 1 and 2 to rest against the inwardly extending edge that extended inwards of Object 2. This tended to detach the surface of Fingertip 2 from the side wall of Object 2, so that they were not parallel to each other. This reduced the contact area, and the characteristics obtained corresponded to those received for Objects no. 1 and 3 where the contact occurred at the edge. Due to the flat wall surface of Object 2, contact was maintained over a longer distance compared to Objects 1 and 3. Object no. 3 obtained the highest values of pulling force, and the waveforms were similar to Object no. 1 in their shape. During movement, it was in contact with the edge of the hexagon occurring in the cross section. As discussed above, decreases in the force values for Fingertip types 1 and 2 with an object displacement was caused by the presence of static and kinetic friction; however, it is also worth noting that the authors proposed circular overlays corresponding to a cushion base with a diameter of 25 mm. Due to this shape, the displacement along the axis perpendicular to the surface of the overlay successively reduced its contact area with the object. From a position of length equal to the diameter of the circle, this segment changed to a chord. Its length, in turn, depended on the offset from the center of this circle. In the case of classic, rigid fingertips, the contact of their surface with a grasped object is made along its edge or sidewall, and design considerations of the gripper can cause an expected parallelism of the fingertips to the object not to be met as was the case with Object no. 2. This is worth considering when analyzing soft fingertips. Adaptive soft structures will adapt to the shape of an object being grasped, and in the case of rigid structures, a translation or rotation of the object can positively or negatively affect the stability of the grasp. Here, the last important observation was the visible scratch on Fingertip 2 caused by contact of the friction pair.

3.2. Fingertip Type 3

The characteristics of the soft cushions differed in terms of their shape and the values obtained from the pull-out forces of the objects with the fingertips, which were smaller. The phenomenon described in Section 2.5 and shown in Figure 6 in Stage 2—fixing and Stage 3—pulling-out was seen. In most cases, the characteristics began with an increase in force that gently progressed to a peak along an arc (Figure 8). This was due to the need for movement to fix the slack created when the jaws were tightened. The exception was Object no. 3 for Fingertip type 3A where the movement at the top was jerked along the length of its pull-out. The geometry of the cushions found in Fingertip type 3A was characterized by thinner walls compared to Fingertip type 3B. Thinner cushions exhibited a greater flexibility expressed by less force required to deform them; however, the authors observed their tendency to ripple in the apex region. A spiral formation using 3D printing stiffened the structure at the tip because of the decreasing radius of the layer as the vault of the hemisphere closed. This phenomenon was not observed for the fingertips with MRFs using this geometry (i.e., Fingertip types 4A and 4C). In the process of closing and releasing air from them according to Figure 4, the tip was sucked inside the cushion. For Object no. 1, higher force values were observed for Fingertip type 3B. A large influence in this case was the increasing cross-section of the cushion walls at its base. This was especially effective for jaw clamping and the first stages of movement; however, it is worth noting Fingertip type 3A, due to its flexibility, was capable of achieving higher force values when moving the object further. For example, for a displacement distance of Object no. 1 equal to 10 mm, the Fingertip type 3A reached values around 9 N and the Fingertip type 3B around 7 N. The benefits of a flexible structure were even more apparent in the case of Object no. 2. The ability to maintain higher force values over a longer displacement was exhibited by the Fingertip type 3A. As was seen, passive cushion structures, capable of adapting to the shape of an object being grasped, tend to offer gentle resistance to pull the element out of its compression. Removing the rigid jaw structure in the process results in a reduction in the maximum force values achieved during movement.

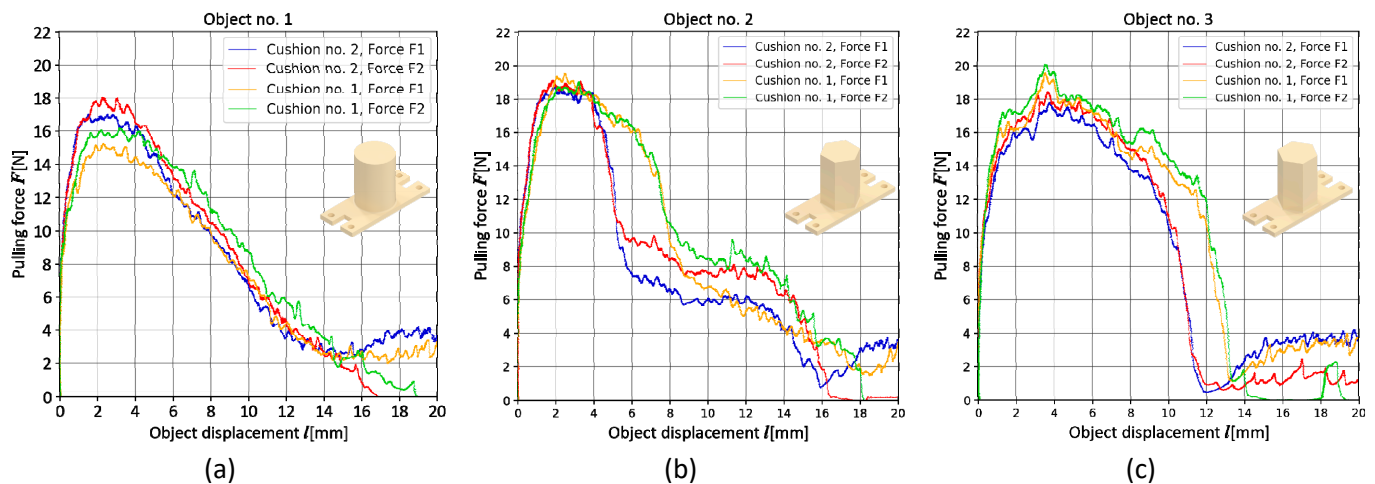


Figure 8. Measurement of the pulling force of an object from Cushions no. 1 (Fingertip type 3A) and 2 (Fingertip type 3B) as a function of its displacement for: (a) Object no. 1; (b) Object no. 2; (c) Object no. 3.

3.3. Fingertip Type 4

Due to the apparent potential in the application of MRF, the authors decided to compare cushions in several configurations in terms of filling. These were discussed in Section 2.3. The studies for individual MR cushions were realized for the case of an insertion of a magnetic field and its absence. This made it possible to evaluate the effect of using a smart fluid. The penetration of the cushion into the object was carried out each time in the absence of a magnetic field. Figure 9 shows the percentage increase in the maximum pulling

force after insertion of the magnetic field for the individual cushions. The source of the magnetic field in each case was a $\varnothing 29 \times 8$ mm magnetic holder (with a $\varnothing 24 \times 4$ magnet). Among those with MRF, Cushions no. 5 and 6 were the least responsive, with both using the same RHEOTEC+ fluid; however, based on the test, the authors selected Cushions no. 3 and 8 with fluid from the LORD company [29]. In their case, it was observed that the value of the force required to pull the objects was even doubled. With holding the first, Cushion no. 8 minimally performed better. With the second, Cushion no. 3 dominated. Object no. 3 was satisfactory for both cushions, which adapted very well to its shape, as intended. It should be clearly mentioned that Cushion no. 7 with the RHEOTEC+ fluid also performed relatively well. While the percentage change due to the insertion of the magnetic field was comparable, it is worth noting the difference in the maximum pull-out forces that were obtained. This aspect will be discussed in the following discussion.

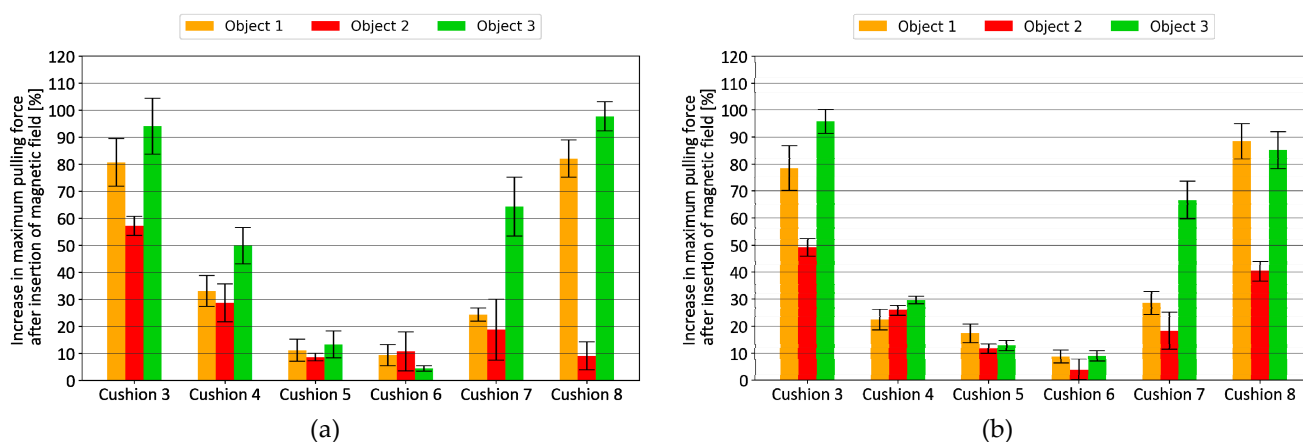


Figure 9. Increase in the maximum pulling force after insertion of the magnetic field (%): (a) force F1; (b) force F2.

Given the insights from the data in Figure 9., the waveforms for the selected cushions that performed best in the conducted tests are shown in Figure 10. This is a summary of the cushions with MRFs measurements, which were based on geometries with thinner walls and a rigid fingertip (i.e., type 2). In most cases, Cushion no. 8 achieved the highest values of object pulling force of all the fingertips. The exception was Object no. 2 for force F1 (Figure 10b). It is worth noting that it is not always the case that increasing the jaw force increases the pulling force of objects, and information on the ability of jaws to hold specific shapes at different actuation force parameters allows for the selection of a variable gripping strategy, adapted to the geometry of the object to be gripped. Here, the cushions with MRF performed best with Object no. 3. The triangular prism penetrated deep into the cushion and adapted to its shape. This stiffened the filling by inserting a magnetic field to effectively hold this object. Object no. 1 appeared to have a too-large cross-sectional diameter to use for a small cushion. By comparing the results, therefore, it can be concluded that the soft fingertips can perform on the same level as the rigid ones under the same conditions.

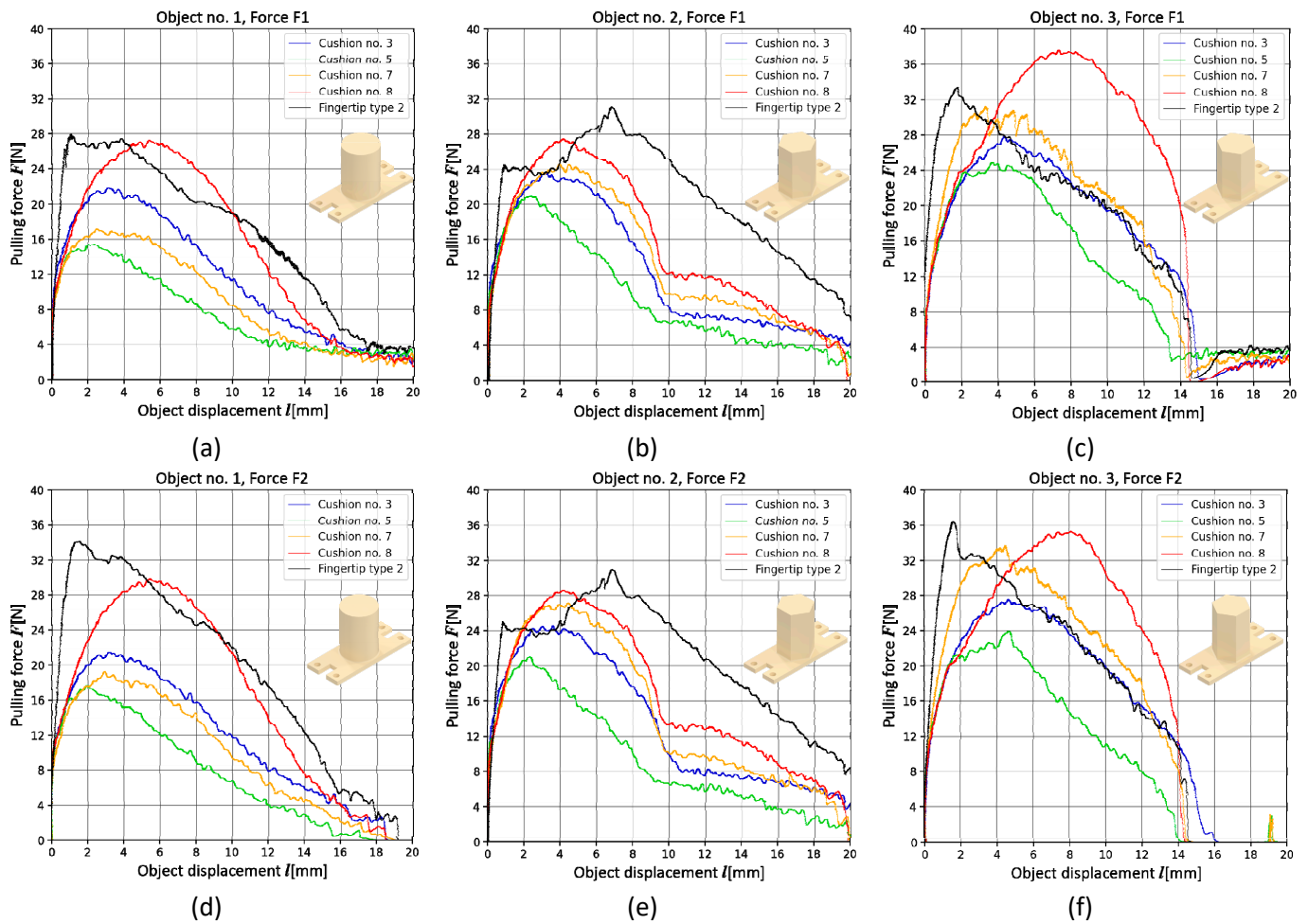


Figure 10. Comparison of measurements of the pulling force of an object from Cushions no. 3, 5, 7 and 8 when a magnetic field is applied and Fingertip type 2 as a function of its displacement for: (a) Object no. 1, with jaw force F1; (b) Object no. 2, with jaw force F1; (c) Object no. 3, with jaw force F1; (d) Object no. 1, with jaw force F2; (e) Object no. 2, with jaw force F2; (f) Object no. 3, with jaw force F2.

4. Discussion

The advantage of the MRF cushion is its ability to adapt to the shape of the grasped object. Figure 11 summarizes the research and introduces an indicator of the object’s pull-out force along the length of its displacement.

The authors proposed a factor f_g :

$$f_g = \sum_{i=0} F_i \cdot l_i \tag{1}$$

that is the sum of the product of the gripper force F_i and the distance of the prism displacement l_i (Figure 11). Thus, its result considers not only the maximum value of the force but also the extent of the surface area on which it was acting, especially the appearance of a large force while moving the object (i.e., increasing the object displacement l). This would not happen if one counted the integral as a field under the graph. Figure 11 shows its value for each fingertip with an indication of the maximum pull-out force obtained and the results should be compared within each object. For example, in Figure 10, each object is characterized by different contact lengths of the fingertips.

Figure 10 shows the particular advantage of the MRF-140CG fluid cushions. As studies have shown, the use of the same magnetic field source does not guarantee the same effects for different fluids and fillings, and as mentioned earlier, the highest values among the

soft samples here were achieved by Cushion 8. The use of microbeads is a significant improvement in this application. As shown in Figure 9, this is a modification achieved with a notable difference considering the behavior of the cushion in the absence and presence of a magnetic field. Thus, it should be borne in mind that the use of MRFs in grippers involves modifications to improve their properties. This application is quite different from the original use of MRF in clutches, shock absorbers, or brakes, for example. The liquid supplied by manufacturers is not suitable for application in a gripper and must, therefore, be modified. This is evidenced in Figure 9, which summarizes the effect of inserting a magnetic field inside the cushion. For Cushions 5 and 6, the difference was negligible considering the error bars.

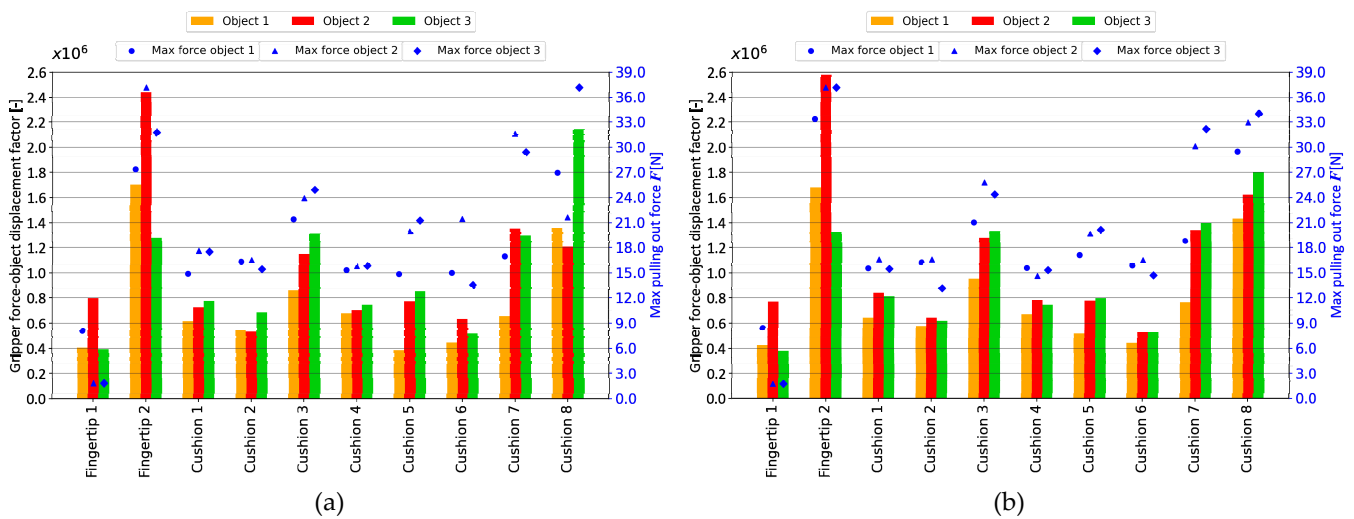


Figure 11. Maximum gripper force-displacement factor for each cushion with a maximum gripper force: (a) force F1; (b) force F2.

It is worth noting that all the cushions were characterized by a smooth transition to the value of a maximum pull-out force. This also demonstrated the gentle displacement of the object in the jaws. On the one hand, this is a desirable effect, which makes it possible to perform small displacements, that are crucial in terms of the task at hand. In the case of rigid jaws, there is friction, which blocks the possibility of such movements and changing the orientation inside the grip can damage the surface of the jaws and the object being held; however, the possibility of movement inside the cushioned jaws can be a negative feature. This will especially be the case when the object being held cooperates with another one. An example is inserting a screw held in the pressure of jaws into a hole and it may be that the screw will turn in the gripper cushions. The human hand is not perfect and behaves in the same way; therefore, tools such as screwdrivers or wrenches are used. The same applies, for example, to opening jars.

5. Conclusions

The work proposed jaws using MR fluid and described the process of their preparation and the research presented the authors' stand and methodology for measuring gripping force. In their opinion, the presented measurement method is reproducible, and thus, is effective in comparative studies. Accordingly, rigid and soft fingertips have been prepared. The study was carried out on three objects characterized by a different shape and the results of each measurement were presented and discussed. Rigid fingertips use only a frictional force that affects the surface of the interacting parts. Cushions, on the other hand, provide resistance to moving the component using their geometry, stiffness and filling. Passive cushion structures, capable of adapting to the shape of the object being grasped, tend to offer gentle resistance to pull the element out of their compression and the proposed *fg* factor promotes jaws that

maintain a high pull-out force when moving an object inside them. The use of small-sized cushions made it possible to use a small amount of fluid, and thus, the possibility of control with a smaller magnetic field source. Modifying the fluid by increasing its density or mixing it with microbeads allows for obtaining significantly better results. Cushions with MRF work best with Object no. 3, which is the triangular prism. As shown, MRF cushions can compete with rigid jaws considering the payload gained. Moreover, consider their adaptability, examples of their applications include handling elements made of glass with small dimensions and various shapes on production lines, transporting electronic components and modules, and picking fruit in the agricultural industry.

The solutions proposed in the article will be developed to grip and move fragile objects that could easily be damaged. In the next steps, the authors will conduct research related to control and object relocation with the solution proposed here.

Author Contributions: Conceptualization, M.B. and D.R.; methodology, M.B.; software, D.R. and M.B.; validation, M.B. and D.R.; formal analysis, M.B.; investigation, M.B.; resources, M.B.; data curation, M.B.; writing—original draft preparation, M.B.; writing—review and editing, D.R.; visualization, M.B.; supervision, D.R.; project administration, M.B.; funding acquisition, M.B. All authors have read and agreed to the published version of the manuscript.

Funding: This research was funded in whole by the National Science Centre, Poland grant number: 2021/41/N/ST8/02619. For the purpose of Open Access, the author has applied a CC-BY public copyright licence to any Author Accepted Manuscript (AAM) version arising from this submission.

Institutional Review Board Statement: Not applicable.

Informed Consent Statement: Not applicable.

Data Availability Statement: The authors are eager to share the results obtained and encourage contact with the corresponding author.

Conflicts of Interest: The authors declare no conflict of interest.

References

1. Terrile, S.; Argüelles, M.; Barrientos, A. Comparison of Different Technologies for Soft Robotics Grippers. *Sensors* **2021**, *21*, 3253. [[CrossRef](#)] [[PubMed](#)]
2. Hughes, J.; Culha, U.; Giardina, F.; Guenther, F.; Rosendo, A.; Iida, F. Soft Manipulators and Grippers: A Review. *Front. Robot. AI* **2016**, *3*, 69. [[CrossRef](#)]
3. Manti, M.; Hassan, T.; Passetti, G.; d'Elia, N.; Cianchetti, M.; Laschi, C. An Under-Actuated and Adaptable Soft Robotic Gripper. In *Biomimetic and Biohybrid Systems*; Wilson, S.P., Verschure, P.F.M.J., Mura, A., Prescott, T.J., Eds.; Lecture Notes in Computer Science; Springer International Publishing: Cham, Switzerland, 2015; Volume 9222, pp. 64–74, ISBN 978-3-319-22978-2.
4. Yan, J.; Xu, Z.; Shi, P.; Zhao, J. A Human-Inspired Soft Finger with Dual-Mode Morphing Enabled by Variable Stiffness Mechanism. *Soft Robot.* **2022**, *9*, 399–411. [[CrossRef](#)] [[PubMed](#)]
5. Liu, C.-H.; Chen, L.-J.; Chi, J.-C.; Wu, J.-Y. Topology Optimization Design and Experiment of a Soft Pneumatic Bending Actuator for Grasping Applications. *IEEE Robot. Autom. Lett.* **2022**, *7*, 2086–2093. [[CrossRef](#)]
6. Xiao, W.; Liu, C.; Hu, D.; Yang, G.; Han, X. Soft Robotic Surface Enhances the Grasping Adaptability and Reliability of Pneumatic Grippers. *Int. J. Mech. Sci.* **2022**, *219*, 107094. [[CrossRef](#)]
7. Yang, L.; Han, X.; Guo, W.; Wan, F.; Pan, J.; Song, C. Learning-Based Optoelectronically Innervated Tactile Finger for Rigid-Soft Interactive Grasping. *IEEE Robot. Autom. Lett.* **2021**, *6*, 3817–3824. [[CrossRef](#)]
8. Cai, L.; Dong, S.; Huang, X.; Fang, H.; She, J. Mechanical Performance Analysis and Experimental Study of Soft-Bodied Bird-Billed Pneumatic Gripper. *Ind. Robot.* **2022**, *49*, 924–933. [[CrossRef](#)]
9. Hughes, J.; Li, S.; Rus, D. Sensorization of a Continuum Body Gripper for High Force and Delicate Object Grasping. In Proceedings of the 2020 IEEE International Conference on Robotics and Automation (ICRA), Paris, France, 31 May–31 August 2020; pp. 6913–6919.
10. Zhang, P.; Chen, W.; Tang, B. Design and Feasibility Tests of a Lightweight Soft Gripper for Compliant and Flexible Envelope Grasping. *Soft Robot.* **2022**, *9*, 376–385. [[CrossRef](#)]
11. Mathew, B.P.; Devasia, F.; Asok, A.; Jayadevu, P.R.; Baby, R. Implementation of an Origami Inspired Gripper Robot for Picking Objects of Variable Geometry. *Mater. Today Proc.* **2022**, *58*, 176–183. [[CrossRef](#)]
12. Li, S.; Lin, J.; Kang, H.; Cheng, Y.; Chen, Y. Bio-Inspired Origamic Pouch Motors with a High Contraction Ratio and Enhanced Force Output. *Robot. Autom. Syst.* **2022**, *149*, 103983. [[CrossRef](#)]
13. Białek, M.; Jędrzycka, C.; Milecki, A. Investigation of Thermoplastic Polyurethane Finger Cushion with Magnetorheological Fluid for Soft-Rigid Gripper. *Energies* **2021**, *14*, 6541. [[CrossRef](#)]

14. Hong, S.-W.; Yoon, J.-Y.; Kim, S.-H.; Lee, S.-K.; Kim, Y.-R.; Park, Y.-J.; Kim, G.-W.; Choi, S.-B. 3D-Printed Soft Structure of Polyurethane and Magnetorheological Fluid: A Proof-of-Concept Investigation of Its Stiffness Tunability. *Micromachines* **2019**, *10*, 655. [CrossRef] [PubMed]
15. Korger, M.; Glogowsky, A.; Sanduloff, S.; Steinem, C.; Huysman, S.; Horn, B.; Ernst, M.; Rabe, M. Testing Thermoplastic Elastomers Selected as Flexible Three-Dimensional Printing Materials for Functional Garment and Technical Textile Applications. *J. Eng. Fibers Fabr.* **2020**, *15*, 1558925020924599. [CrossRef]
16. Nihal, R.A.; Broti, N.M.; Deowan, S.A.; Rahman, S. Design and Development of an Anthropomorphic Robotic Hand Using TPU Material. In Proceedings of the 2019 2nd International Conference on Innovation in Engineering and Technology (ICIET), Dhaka, Bangladesh, 23–24 December 2019; pp. 1–6.
17. Balak, R.; Mazumdar, Y.C. Bistable Valves for MR Fluid-Based Soft Robotic Actuation Systems. *IEEE Robot. Autom. Lett.* **2021**, *6*, 8285–8292. [CrossRef]
18. Somlor, S.; Aguirre Dominguez, G.; Schmitz, A.; Kamezaki, M.; Sugano, S. A Haptic Interface with Adjustable Stiffness Using MR Fluid. In Proceedings of the 2015 IEEE International Conference on Advanced Intelligent Mechatronics (AIM), Busan, Korea, 7–11 July 2015; pp. 1132–1137.
19. Nishida, T.; Okatani, Y.; Tadakuma, K. Development of Universal Robot Gripper Using MR α Fluid. *Int. J. Human. Robot.* **2016**, *13*, 1650017. [CrossRef]
20. Tsugami, Y.; Barbie, T.; Tadakuma, K.; Nishida, T. Development of Universal Parallel Gripper Using Reformed Magnetorheological Fluid. In Proceedings of the 2017 11th Asian Control Conference (ASCC), Gold Coast, QLD, Australia, 17–20 December 2017; pp. 778–783.
21. Cramer, J.; Cramer, M.; Demeester, E.; Kellens, K. Exploring the Potential of Magnetorheology in Robotic Grippers. *Procedia CIRP* **2018**, *76*, 127–132. [CrossRef]
22. Pettersson, A.; Davis, S.; Gray, J.O.; Dodd, T.J.; Ohlsson, T. Design of a Magnetorheological Robot Gripper for Handling of Delicate Food Products with Varying Shapes. *J. Food Eng.* **2010**, *98*, 332–338. [CrossRef]
23. Hartzell, C.M.; Choi, Y.T.; Wereley, N.M.; Leps, T.J.G. Performance of a Magnetorheological Fluid-Based Robotic End Effector. *Smart Mater. Struct.* **2019**, *28*, 035030. [CrossRef]
24. Naimzad, A.; Ghodsi, M.; Hojjat, Y.; Maddah, A. MREs Development and Its Application on Miniature Gripper. *Proc. Int. Conf. Adv. Mater. Eng.* **2011**, *15*, 75–80.
25. Skfivan, V.; Sodomka, O.; Mach, F. Magnetically Guided Soft Robotic Grippers. In Proceedings of the 2019 2nd IEEE International Conference on Soft Robotics (RoboSoft), Seoul, Republic of Korea, 14–18 April 2019; pp. 126–130.
26. Choi, Y.T.; Hartzell, C.M.; Leps, T.; Wereley, N.M. Gripping Characteristics of an Electromagnetically Activated Magnetorheological Fluid-Based Gripper. *AIP Adv.* **2018**, *8*, 056701. [CrossRef]
27. Liu, Q.; Jing, T.; Mo, A.; Xu, X.; Zhang, W. A Novel Robot Hand with the Magneto-Rheological Fluid Solidification. In Proceedings of the 2015 IEEE International Conference on Robotics and Biomimetics (ROBIO), Zhuhai, China, 6–9 December 2015; pp. 2495–2500.
28. Wang, Y.; Yang, Z.; Zhou, H.; Zhao, C.; Barimah, B.; Li, B.; Xiang, C.; Li, L.; Gou, X.; Luo, M. Inflatable Particle-Jammed Robotic Gripper Based on Integration of Positive Pressure and Partial Filling. *Soft Robot.* **2022**, *9*, 309–323. [CrossRef] [PubMed]
29. LORD MRF-140CG Documentation Site. Available online: https://lordfulfillment.com/pdf/44/DS7012_MRF-140CGMRFluid.pdf (accessed on 20 December 2022).
30. Arus MR Tech RHEOTEC+ Documentation Site. Available online: <https://arusmrtech.com/wp-content/uploads/2021/11/RHEOTEC.pdf> (accessed on 20 December 2022).
31. PrusaSlicer Site. Available online: https://www.prusa3d.com/page/prusaslicer_424/ (accessed on 20 December 2022).
32. Turekova, I.; Szabova, Z.; Chrebet, T.; Harangozo, J. The Effect of External Conditions on Ignition Temperature of Thermoplastic Polyurethane Elastomers. *Adv. Mater. Res.* **2013**, *838–841*, 14–17. [CrossRef]
33. B&R Site. Available online: <https://www.br-automation.com/> (accessed on 20 December 2022).

Disclaimer/Publisher’s Note: The statements, opinions and data contained in all publications are solely those of the individual author(s) and contributor(s) and not of MDPI and/or the editor(s). MDPI and/or the editor(s) disclaim responsibility for any injury to people or property resulting from any ideas, methods, instructions or products referred to in the content.